Compressive Strength Parallel to the Grain in Relation to Moisture Content in *Calamus simplicifolius* Cane

Limei Yang Xing'e Liu Zehui Jiang Genlin Tian
Shumin Yang Lili Shang

Abstract

This research aimed to investigate the compressive fracture behavior and the compressive strength parallel to the grain in relation to moisture contents (MC) below and above the fiber saturation point (FSP) in *Calamus simplicifolius* cane. FSP of the rattan was investigated using a dynamic vapor sorption (DVS) apparatus, and the fracture behaviors of compression parallel to grain were analyzed by three-dimensional X-ray microcomputed tomography. The study indicated that the value of FSP derived from the DVS method was 25 percent. The average compressive strength parallel to the grain was found to be 39 MPa at 3 percent MC, 30 MPa at 10 percent MC, 17 MPa at 12 percent MC, 12 MPa at 27 percent MC, and 10 MPa at 45 percent MC. The strains of the yield and densification stage were prolonged with increasing MC, whereas the stress in the linear elastic stage decreased with increasing MC. The cracks of the rattan core and the deflection angle at higher MC were larger than that of low MC. Below the FSP, the compressive failure of the rattan showed a shear band oriented around 45° to the loading axis, and the surface was rough. Above the FSP, the rattan samples showed brooming failure. The interface among fiber bundles was delaminated and the fiber surface in the failure area was smooth. The fracture toughness of the rattan was higher than that of wood, which suggests that the rattan might be more suitable for modeling and curved materials.

"Rattan" is a collective term that refers to spiny climbing palms belonging to the subfamily Calamoideae of the family Palmae and those classified under the subfamily Calamoideae of the family Arecaceae. It is comprised of 13 genera and more than 600 species that are mainly distributed in tropical and subtropical regions (Liese and Walter 2003). *Calamus simplicifolius* is an important commercial rattan species in China because of its superior mechanical properties, and could act as a substitute material for traditional forest products and structural materials. The stem of *C. simplicifolius* is anatomically structured by longitudinal vascular bundles that are unevenly embedded in a matrix of parenchyma tissue. Each vascular bundle consists of one metaxylem vessel, two phloem fields, and three or four protoxylem tracheids (Fig. 1b). The metaxylem vessel is the largest cell in *C. simplicifolius*, with an average diameter of 288 μm (Wang et al. 2019). These voids can be easily penetrated by any surrounding water and water vapor during processing and service.

It is well known that moisture content (MC) has an important influence on the physical and mechanical properties of wood and bamboo. Rattan cane, like wood and bamboo, is a hygroscopic material, which means that it absorbs and exchanges water molecules with its surroundings. Rattan and rattan derivatives are quite sensitive to MC (Wang 2015), given that there are large numbers of exposed hydrophilic groups (e.g., hydroxyl) at the macromolecule surfaces (Youssefian and Rahbar 2015). It is difficult to stress the critical role of water in each segment in the processing and use of rattan (Luo et al. 2012). So far, limited research has examined the relationship between the mechanical properties and MC in the rattan. Shang (2014) reported that the MC had a significant effect on the fracture toughness of cracks prefabricated from the rattan cores and that the fracture toughness in the air-dried condition was significantly higher than that in the saturated-water condition. However, the study did not explain the difference.

In general, the fiber saturation point (FSP), which was originally defined by Tiemann (1906), refers to the absence

The authors are, respectively, Doctor, Researcher, Professor, Research Assistant, Researcher, and Research Assistant, Key Lab. of Bamboo and Rattan Sci. and Technol. of the State Forestry Admin., Dept. of Bio-Mater., International Center for Bamboo and Rattan, Beijing (18811717626@163.com, liuxinge@icbr.ac.cn, jiangzehui@icbr.ac.cn [corresponding author], tiangenlin@icbr.ac.cn [corresponding author], yangsm@icbr.ac.cn, shangll@icbr.ac.cn). This paper was received for publication in November 2019. Article no. 19-00061.

Forest Prod. J. 70(3):309–316.
doi:10.13073/FPJ-D-19-00061

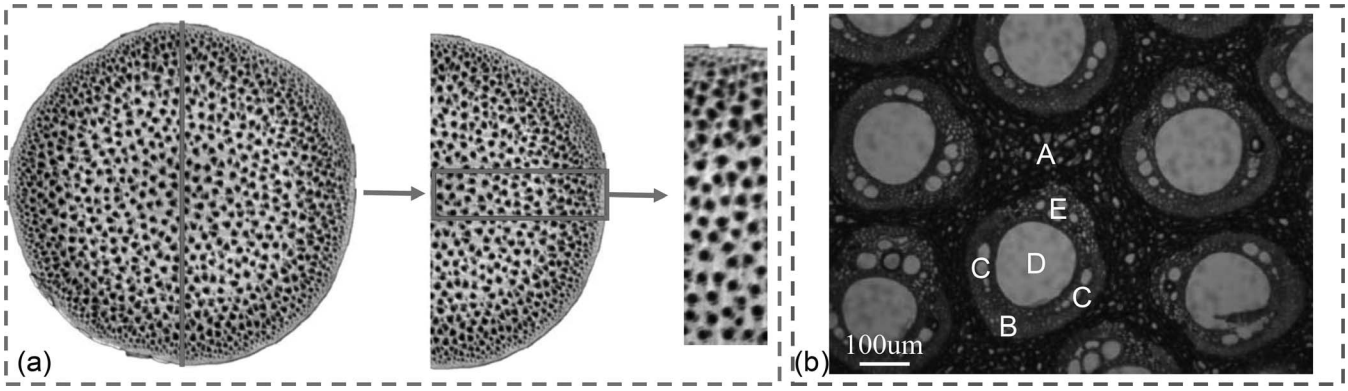

Figure 1.—(a) Rattan sample used in the experiment. (b) Optical microscopy image of the cross-section of Calamus simplicifolius. *(A) Parenchyma tissue, (B) fibrous sheath, (C) phloem fields, (D) metaxylem vessel, and (E) protoxylem tracheids.*

of any free water in the cell lumen, whereas the cell walls are saturated with chemically and physically bound water. Practically, the FSP has been considered as the MC above which the physical and mechanical properties of wood no longer change as a function of MC (Simpson and TenWolde 1999). Liu et al. (2014a) found that the bending properties of *Daemonorops margaritae* cane were closely related to MC. The modulus of elasticity and modulus of rupture declined significantly with increasing MC below the FSP.

Compressive strength is one of the important mechanical properties of wood. Studies (Irby et al. 2020a, Verbist et al. 2020) show that the wood compressive strength is linearly correlated with wood density. However, the correlation between wood compression strength and rings per inch is only slightly significant (Irby et al. 2020b). The compression strength can be predicted accurately by the regression models (Christoforo et al. 2020). For practical purposes, such as using wood as a construction material, the MC is one of the important factors affecting the compression performance (Aicher and Stapf 2016). Axial compression is also one critical characteristic that determines the suitability and performance of rattan for different structural applications. The resistance to compression in the rattan cane samples has been found to be proportional to the volume fraction of vascular bundles in the cross-section (Liu et al. 2014b). However, few studies in the literature have quantified the compressive properties of rattan in relation to MC. Furthermore, the corresponding compression failure modes of rattan under different MCs have not yet been investigated.

The aim of the present study was to examine the relationship between compressive strength and MC in *C. simplicifolius* cane. The water adsorption/desorption and FSP of rattan were determined by the dynamic vapor sorption (DVS) technique. In addition, the compression deformation and the failure behaviors in the rattan cane were also analyzed by three-dimensional X-ray microcomputed tomography (CT). A better understanding of the rattan compression strengths in relation to MC will contribute to better processing and utilization of the rattan resource.

Materials and Methods

Materials and sample preparation

Rattan (*C. simplicifolius*) canes with an average diameter of 20 mm were collected from a plantation located in Pingxiang City, Guangxi Province, China. All samples were cut from a height of 30 cm above the ground, and every five internode samples were obtained and labeled from each of the stems.

Rattan stems develop from the apical meristem, which results in the occurrence of the youngest tissue toward the top of the stem and the oldest toward the bottom (Rich 1986). It was difficult to determine the age of rattans because of the absence of annual growth rings. Cylindrical sample pieces (diameter 20 mm, length 5 mm) were taken from the middle portion of the rattan stem for DVS tests (Fig. 2). To minimize the rattan variability caused by the hierarchical architecture with vascular bundles nonuniformly distributed along the radial direction, small rattan blocks (around 35 mg) containing the waxy epidermises and rattan core with dimensions of 1 by 3 by 3 mm^3 (thickness by length by width) were prepared from the rattan block (Fig. 1).

The samples for the compression strength tests were cut from the middle internodes. The length (L)-to-diameter (D) ratio of the samples was 2:1 to avoid buckling failure during the compression test, and the upper and lower end surfaces of each sample had to be parallel and vertical to the center line of the sample (Liu et al. 2014b; Fig. 2). Four-fifths of the samples were placed in desiccators containing saturated salt solutions for 2 months before the compression tests until the weight difference reached to less than 0.1 percent in a 24-hour interval (Esteban et al. 2015), as listed in Table 1. The last fifth of the samples was accurately dehydrated to absolute dry in a temperature-controlled oven (water weight content of 0%), and then soaked in distilled water and

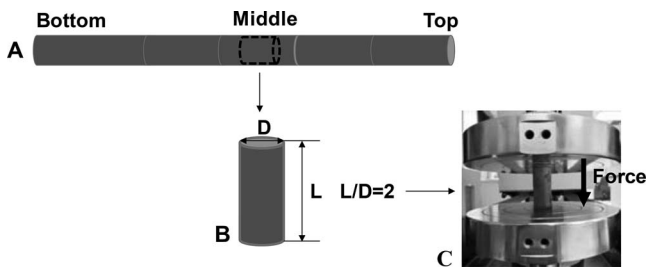

Figure 2.—Schematic of compression sample preparation. (A) Samples cut from the middle position of the rattan cane; (B) length (L)-to-diameter (D) ratio of the samples (2:1); (C) compression parallel to the grain.

Table 1.—Saturated salt solutions and relative humidity.

Salt	Temperature (°C)	Relative humidity (%)	Actual humidity (%)
LiBr	20	6.4 ± 0.6	3
$MgCl_2$	20	32.8 ± 0.2	10
NaCl	20	75.3 ± 0.2	12
KCl	20	84.2 ± 0.3	27
Deionized water	20	—	45

measured every 2 hours until the water content reached up to 45 percent. Samples with different MCs were obtained, and at least 20 samples at each MC level were selected for subsequent testing.

Methods

DVS setup.—A DVS apparatus (DVS Intrinsic; Surface Measurement Systems Ltd., UK) was used to determine the isotherm behavior of the rattan canes. Each sample was placed into a clean sample basket connected to the microbalance. There was a constant flow of dry nitrogen gas through the climate-controlled chamber where another flow of nitrogen-containing water vapor was mixed to maintain a given relative humidity (RH) value at a constant temperature of 25°C (Keating et al. 2013). The RH increased from 0 to 95 percent in step sequences of 10 percent and then decreased to 0 percent RH in reverse order. The samples in the instrument were maintained at a constant RH until the weight change was less than 0.002 percent per 10 minutes. Data on the weight change were acquired every 20 seconds (Čermák et al. 2016), and the data obtained by the DVS technique were highly reproducible (Xie et al. 2011).

Axial compression test.—The compression strength was measured with a universal mechanical tester (5582 Instron Co., USA) according to the standard GB/T 1935-2009 (Standardization Administration of China 2009). The loading speed was 6 mm min^{-1} and the testing time was 60 ± 30 seconds.

Characterization of compression failure behaviors.—The three-dimensional X-ray micro-CT (nano Voxel 2000; Sanying Precision Instruments Co., Ltd., China) was used to observe internal structure changes of the damaged samples in detail.

Sections of the failure surfaces were collected from the tested samples at different MCs by a blade and frozen in liquid nitrogen to preserve the primitive fracture morphology. The compression failure surfaces were observed by a field-emission scanning electron microscope (FE-SEM; XL30; FEI, USA) with an operating voltage of 7.0 kV.

Results and Discussion

Rattan hygroscopicity

Equilibrium moisture content (EMC) is an important parameter for characterizing water vapor adsorption and desorption isotherms of lignocellulose materials. As presented in Figure 3a, the isotherm of the rattan exhibits sigmoidal isotherms in adsorption processes. It belongs to the type II defined by Brunauer et al. (1940). From the inset in Figure 3a, the slope of RH from 0 to 5 percent is lower than the slope from 5 to 10 percent because of stronger sorbate–adsorbent interactions, leading to monolayer formation (Bedane et al. 2014). The EMC exhibits an upward bend when the RH is above 80 percent, whereas the desorption isotherm is linear at the same RH levels. The results are similar to those of wood (Hill et al. 2012). According to the definition of FSP (Tiemann 1906, Skaar 1988), the EMC of the rattan at 100 percent RH is 25 percent (Table 2). The EMC value of *C. simplicifolius* is higher than those of 13 bamboo species ranging from 16 to 24 percent (Zhang et al. 2017). This may be related to the larger porous diameter and higher porous volume of the rattan (Cai et al. 1993) compared with bamboos.

Figure 3a shows that the EMC values at the same RH during the adsorption process are lower than during the desorption process, which displays significant sorption hysteresis in EMC between desorption and adsorption isotherms throughout the hygroscopic range. The sorption hysteresis has been commonly characterized by the absolute hysteresis (Skaar 1988, Walker 2006) and the hysteresis coefficient (Olek et al. 2013). Figure 3b shows that hysteresis increases rapidly from 10 to 70 percent RH and then decreases from 70 to 90 percent RH, which is similar to those of lignin-rich fibers (Hill et al. 2009). The phenomenon of sorption hysteresis can be explained by consideration of the sorption process in a glassy polymer matrix (Hill et al. 2012). During the adsorption process microvoids are created within the matrix, whereas these microvoids collapse during the desorption process (Lu and Pignatello 2004). The hysteresis coefficient is the ratio of the EMC for adsorption to desorption at constant RH (Olek et al. 2013). The hysteresis coefficient of the rattan increases with increasing RH from 10 to 30 percent and then remains almost constant when RH increases further from 30 to 70 percent. Above 70 percent RH, the bond water in the cell wall is saturated, and the hysteresis coefficient increases linearly with increasing RH. The hysteresis coefficient of wood is 0.8 at 0 to 95 percent RH (Liu and Zhao 2004); however, the rattan reaches the same hysteresis coefficient when the RH is close to 80 percent. This may be influenced by the anatomical structure of rattan. Compared with wood, rattan has no radial transfer tissue and cambium (Liu and Zhao 2004), and water is only transported along the longitudinal direction. Therefore, rattan more easily reaches water absorption saturation than wood.

Compression strength parallel to the grain of rattan below and above the FSP

The rattan samples at five MC levels show great differences in the compression performance, as shown in Table 3 and Figure 4. The samples with the lowest MC of 3 percent are brittle and have the highest average compression strength of 39 MPa and the smallest compression strain of 3.7 percent. Samples with MCs of 10 and 12 percent have a similar compression strain, which are 4.9 and 5.1 percent, respectively. Both of the MCs have a more advanced compression strain compared with 3 percent MC. However, the samples with an MC of 10 percent have a better performance in strength (30 MPa) than those with 12 percent MC (17 MPa). A previous study (Liu et al. 2014b) has shown that the compression strength of *Plectocomia assamica* stem is 17.6 MPa at an MC of about 12 percent, which is similar to the results of the present study. As the MC goes up to 45 percent, the compression strength decreases greatly (Fig. 4b). The samples with an MC of 45 percent have an average compression strength of 10

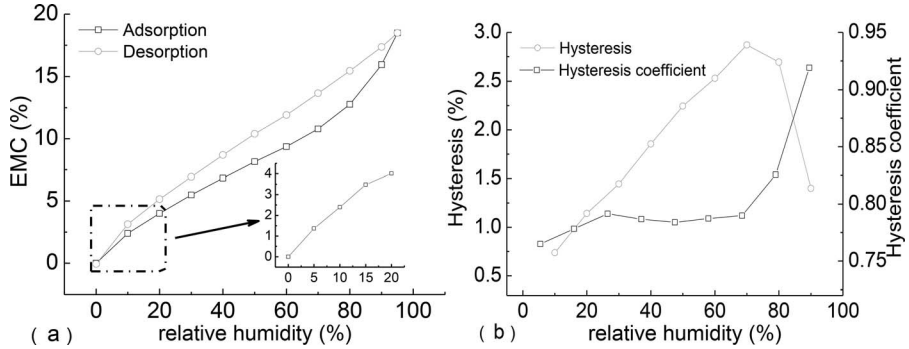

Figure 3.—(a) Equilibrium moisture content (EMC) changes with relative humidity (RH) during the adsorption and desorption processes in the rattan. (b) Hysteresis and hysteresis coefficient in relation to RH in the rattan.

MPa, only about one-fourth that of the samples with the lowest MC, and their compression strain is close to 12.2 percent, which is more than twice as high as that for the samples with 12 percent MC, and is quadruple that of the samples with the lowest MC.

Figure 4a presents the typical stress–strain curves of the rattan at different MCs. The curves for all rattan samples at the five MC levels display a straight segment in the initial phase, followed by a nonlinear plastic phase, which is similar to the pattern in wood (Aicher and Stapf 2016). However, the compressive strength parallel to the grain of rattan is lower than that of wood at the same MC (Aicher and Stapf 2016). The quasiplastic load plateau of the rattan specimens is longer than that of wood, and the slope of stress–strain curves on the descending branch is more gradual than that of wood, which indicates that the toughness of the rattan is higher than that of wood.

Compression fracture behaviors characterized by micro-CT

Figure 5 shows the compression fracture modes parallel to the grain at different MCs. Above the FSP (45% MC), a variety of failure patterns can be observed on the cross-section of the rattan (Figs. 5A1 to 5E1). First, as the load exceeds the maximum strength of vascular bundles in the rattan peel, the vascular bundles on the sample surface in contact with the indenter are separated from the surrounding tissues, as shown in Figure 5A1, and high stress is released. These areas are a linear elastic region in which the strain is directly proportional to the stress (namely the OA1 zone in Fig. 4). When the yield point is reached, the rattan peel separates from the rattan core. The compressive stress is concentrated in the rattan core and the crack (star) is initiated (Fig. 5B1). The crack propagates (arrow) along the parenchyma cell boundaries and the weak interface between the vascular bundles and parenchymatous tissues. It is a plastic region in which the strain increases rapidly with very small or no changes in stress (the A1-to-B1 zone in Fig. 4). The above weak interfaces would allow the crack to grow, inducing a deflection that could reduce the overall damage to the rattan (Figs. 5C1 and 5D1). The slight increase in stress is thought to be a result of the elimination of air voids and the compression of the solid rattan structure. Therefore, this region is termed the densification region (the B1-to-C1 zone in Fig. 4). The range of deflection angle of the crack along the radial direction (RD) in Figures 5C1 and 5D1 is 30° to 135°. Like bamboo (Habibi and Lu 2014), the hollow vessels (metaxylem vessel and protoxylem tracheids) in the rattan cane could lead to additional effects on the crack growth and dissipate its driving energy, or the hollow vessels act as a crack-tip energy absorber to prevent the crack from deflecting. The stress decreases with increasing strain (the C1-to-D1 zone in Fig. 4). The crack-tip energy is completely absorbed and no cracks are observed in Figure 5E1.

Below the FSP (12% MC), cracks develop and the rattan peel separates from the surrounding tissues immediately as the load increases, as shown in Figure 5A2. At this stage, the stress increases sharply with increasing strain (the OA2 zone in Fig. 4) and the stress is widely absorbed by the crack, which could weaken the overall damage to the rattan. The strain increases with a small change in stress (the A2-to-B2 zone in Fig. 4). The failure surfaces decrease gradually along the loading direction (Figs. 5B2 to 5D2). The crack deflection angle (θ) along the RD is estimated to be 0° to 45°. The increase in crack deflection angle consumes a large amount of energy in the crack propagation and prevents the transfer of crack-tip energy. Therefore, the crack disappears in Figure 5E2.

With water absorbed into the rattan samples, the interface dissociation and matrix failure are more sensitive to change in MC. Therefore, the interface dissociation might be the key to the compression strength and toughness of the rattan samples. Above the FSP (45% MC), the cellulose–

Table 2.—Fiber saturation point (FSP) values derived from dynamic vapor sorption (DVS) methods.

Method	Regression equation	R^2	FSP (%)
DVS	$y = 4 \times 10^{-5}x^3 - 0.0044x^2 + 0.2916x - 0.1086$	0.998	25

Table 3.—Compression strength in relation to moisture content (MC) in the rattan.

MC (%)	Compression strength (MPa)
3 (0.32)[a]	39 (3.58)
10 (0.82)	30 (3.82)
12 (0.62)	17 (2.76)
27 (2.95)	12 (2.60)
45	10

[a] Values given in parentheses are the standard deviations ($n = 20$) of the specimens per test.

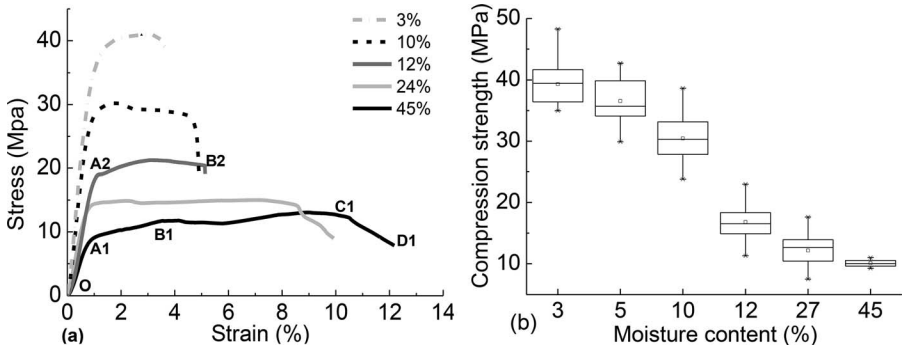

Figure 4.—(a) Stress–strain curves at different moisture contents below and above the fiber saturation point in the rattan. (b) Compression strength parallel to the grain of rattan with different moisture contents.

hemicellulose–lignin complexes swell with the increase of water molecules in the intercellular space. The lubrication of water molecules induces the fiber matrix and the fiber cell wall-to-wall interfaces to easily actuate during the fracture process, which could largely disperse stress and increase the toughness of the rattan. Below the FSP (12% MC), the molecules are close to each other, and the adjacent hydroxyls form hydrogen bonds. The stress concentration cannot be released, and interfacial damages are observed.

As discussed above, the compression-induced cracks could be observed on the fracture surface at MCs both below and above the FSP (Fig. 5). The tortuous cracks originated from the interfaces between the fibers and vessels, or fibers and parenchyma cells, or vessels and paraenchyma cells, and the crack propagation is reduced by metaxylem vessels, phloem fields, protoxylem tracheids, and the pores between parenchyma cells (Habibi and Lu 2014, Wang et al. 2019). The crack propagation kinked at an angle, which could determine the local stress intensity factor through Equation 1 (Hanlon et al. 2005):

$$K_{\text{eff}} = \cos^2(\theta/2)K_{\text{I}} \quad (1)$$

where K_{eff} is the local effective stress intensity factor, θ is the crack deflection angle, and K_{I} is the straight crack growth along the radial direction (Hanlon et al. 2005). Therefore, the K_{eff} among the vascular bundles above (A) and below (B) the FSP are estimated by the following geometric configuration:

$$K_{\text{eff}}^{\text{A}}(R) = (0.15 - 0.93)K_{\text{I}}$$

$$(\theta \in [30^\circ, 135^\circ]), \text{A} \subset 45\%\ \text{MC}$$

$$K_{\text{eff}}^{\text{B}}(R) = (0.85 - 1.00)K_{\text{I}}$$

$$(\theta \in [0^\circ, 45^\circ]), \text{B} \subset 12\%\ \text{MC}$$

The above experimental values validated numerically that the overall effective stress factor at 12 percent MC is higher than that at 45 percent MC. The interfacial cracks occur within the parenchyma tissue as well as honeycomb fibers' bundles (Hanlon et al. 2005). Water brought more hydrogen bonds to the interfaces, making the fiber matrix and the fiber cell wall-to-wall interfaces more lubricated (Chen et al. 2017). Similar phenomena of crack deflections are also found in wood (Valentin and Adjanohoun 1992) and bamboo (Chen et al. 2019). The effective stress intensity factor at 12 percent MC is consistent with Habibi and Lu (2014).

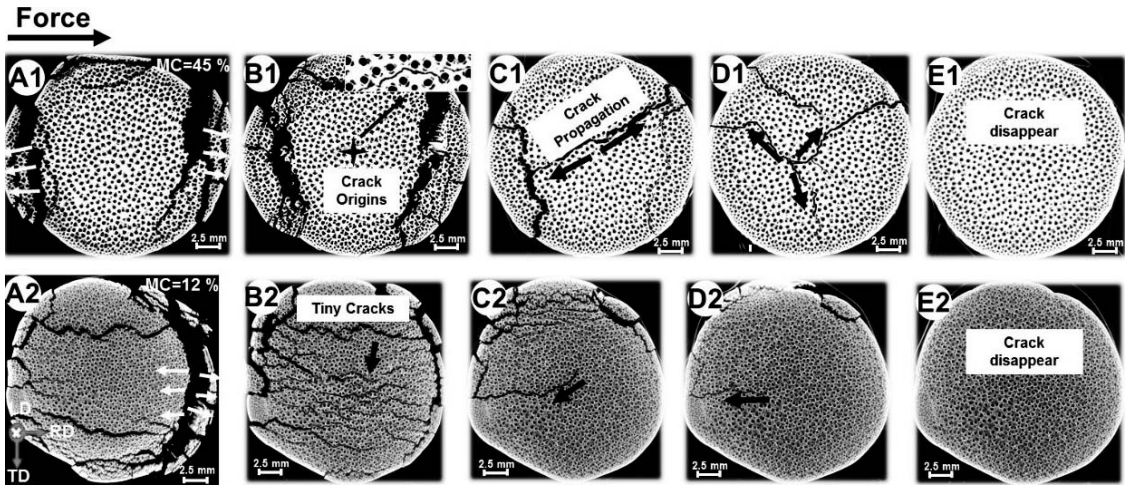

Figure 5.—Failure modes of different layers along the longitudinal compressing of the rattan obtained by three-dimensional X-ray microcomputed tomography. A1 through E1, cross-fracture sections of the wet (45%) samples; A2 through E2, cross-fracture sections of the air-dried (12%) samples.

Fracture microstructural morphologies below and above the FSP

The surface of the compression fracture is observed by an FE-SEM. When the load increased, the ductility of the rattan improved significantly, which may provide more warning of impending failure. This can be primarily attributed to the compressible nature of the parenchyma cells (Fig. 5B1), as these cells behave like foam and can absorb large compressive deformations (Obataya et al. 2007).

According to ASTM D143-94 (American Society for Testing and Materials 2000), the failure modes of rattan compression at different MC levels can be divided into two types. Below the FSP (12% MC), the rattan compressive failure shows a shear band oriented around 45° to the loading axis (Fig. 6A1), and is mainly due to fiber buckling and misalignment, as well as crack initiation and nucleation when the shear band meets the interface of the fiber bundles and parenchyma cells (Fig. 6A2). The fractured parenchyma cells in Figure 6A2 are seriously damaged into chaos, and the cell walls are squeezed to scraps. Fiber bundles near the parenchyma cells are the main load-bearing units and are easily delaminated and ruptured. The delamination is caused by the density differences between the fiber bundles and parenchyma cells (Chen et al. 2019). The fibers are loose and the surface is rough and cracked (Fig. 6A3).

Above the FSP (45% MC), the rattan sample shows brooming failure (Fig. 6B1). The fiber bundles and parenchyma tissue are extruded and bent without a crack appearing between them (Fig. 6B2). However, the interfaces between certain fiber bundles are delaminated, and the fiber bridge could also be found. The fibers with narrow lumens would induce crack deflection, which could decrease the overall damage to rattan in the compressive progress. The fiber surface of the fractured rattan samples above FSP is smoother than that below FSP.

Chen et al. (2017) found that the macrocellular fibrous structures cannot make the bamboo tough and strong without the inner long-chained molecules (cellulose, hemicellulose, and lignin). Like bamboo, rattan is also a cellulose-reinforced composite with special multiscale structures (Bhat et al. 1990, Liu et al. 2014b). The cellulose macromolecular chains in rattan have great influence on strength and toughness. The cell walls of fibers and parenchyma cells mainly consist of cellulose, hemicellulose, and lignin. There are a lot of hydroxyl groups on the surface of cellulose and hemicellulose. Water brought more hydrogen bonds to the fiber matrix and fiber wall-to-wall interfaces, making the interfaces stronger. As a result, the microfiber bridging between two adjacent fibers made rattan with more advanced elongation. As the MC fell, the hydrogen bonding was limited by the separation distances and the encounter opportunities of hydroxyls, where only a few local interfacial damages could be observed and detected.

Conclusions

Using the DVS test method and the three-dimensional X-ray micro-CT, this study examined the hygroscopicity, FSP, and compressive fracture behavior in *C. simplicifolius* cane. The major results can be summarized as follows:

1. Rattan exhibited sigmoidal isotherms in adsorption processes. There was significant sorption hysteresis in EMC between desorption and adsorption isotherms throughout the hygroscopic range. The hysteresis coefficient of 0.8 at 80 percent RH was comparable with that of wood at 0 to 95 percent RH.
2. The FSP value derived from the DVS method was 25 percent. During the compressive progress, the stress–strain curves of the rattan below and above the FSP first displayed an almost linear elastic stage, followed by a nonlinear and plastic change until failure occurred. Compared with wood, the compressive strength parallel to the grain at the same MC was lower in the rattan, but the strain in the plastic stage and the compaction stage was greater. This indicates that the rattan has higher toughness than wood.

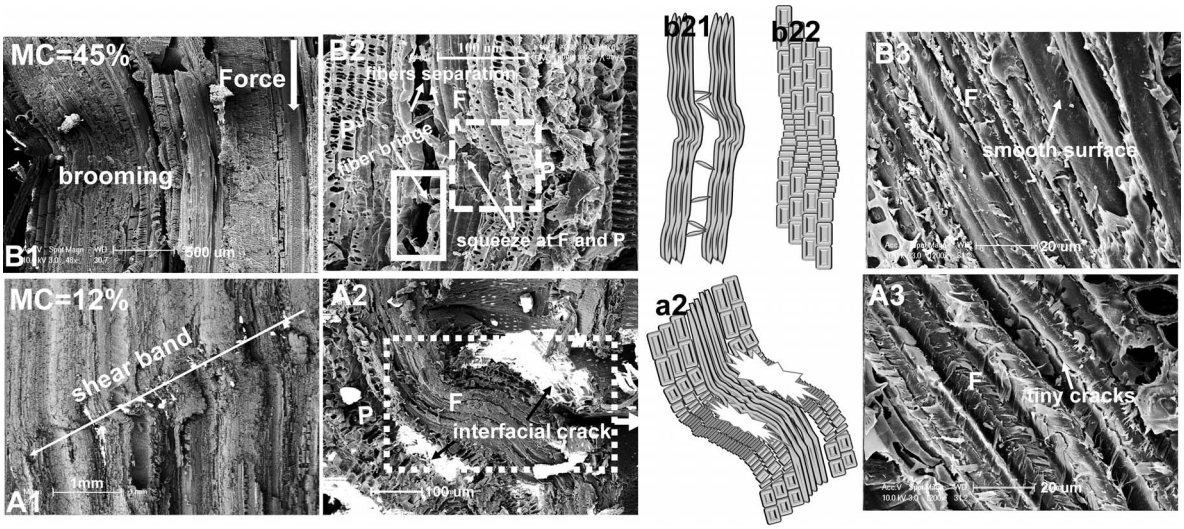

Figure 6.—Scanning electron microscopy morphology of the compression fracture in the radial direction. A1 through A3, longitudinal fracture sections of air-dried (12% moisture content [MC]) samples in different magnifications; B1 through B3, longitudinal fracture sections of wet (45% MC) samples in different magnifications; F = fiber bundles; P = parenchyma; a2 = sketch map of A2 (blue dotted box); b21 = sketch map of fiber delamination and bridge (red dotted box); b22 = sketch map of parenchymal cell squeeze (yellow dotted box).

3. The fiber interfacial areas along with the parenchyma cell boundaries were preferred routes for crack growth in the radial direction. The hollow vessels in the rattan stem also affected the crack propagation by crack deflection or crack-tip energy dissipation.
4. Below the FSP (12% MC), the compressive failure of the rattan showed a shear band oriented around 45° to the loading axis, and the fiber surface was rough and cracked. Above the FSP (45% MC), the rattan samples showed brooming failure. The interface between certain fiber bundles was delaminated. The fibers were bridged and the fiber surface was smooth.
5. The cane with high MC (above 40%) had good flexibility. This suggests that the rattan might be more suitable for applications such as furniture and handicrafts. The growth and reproduction of the staining fungus were closely related to the MC of rattan; therefore, green cane should be dried quickly to below 20 percent MC before storage.

Acknowledgments

The authors gratefully acknowledge the financial support from the National Science and Technology Support Plan (2015BAD04B03) and the National Natural Science Foundation of China (31670565, 31800476).

Literature Cited

Aicher, S. and G. Stapf. 2016. Compressive strength parallel to the fiber of spruce with high moisture content. *Eur. J. Wood Wood Prod*. 74(4):527–542.

American Society for Testing and Materials (ASTM). 2000. Standard test methods for small clear specimens of timber. ASTM D143-94. *In:* ASTM Annual Book of Standards. Wood. ASTM, West Conshohocken, Pennsylvania.

Bedane, A. H., H. N. Xiao, and M. Eic. 2014. Water vapor adsorption equilibria and mass transport in unmodified and modified cellulose fiber-based materials. *Adsorption* 20:863–874.

Bhat, K. M., W. Liese, U. Schmitt, and F. R. G. Hamburg. 1990. Structural variability of vascular bundles and cell wall in rattan stem. *Wood Sci. Technol*. 24:211–224.

Brunauer, S., L. S. Deming, W. E. Deming, and E. Teller. 1940. On a theory of the van der Waals adsorption of gases. *J. Am. Chem. Soc*. 62(7):1723–1732.

Cai, Z. M., Y. Liu, and W. B. Fang. 1993. A study of vessel elements of rattan canes. *Sci. Silvae Sin*. 29(4):293–297. (Translated from Chinese.)

Čermák, P., K. Vahtikari, and L. Rautkari. 2016. The effect of wetting cycles on moisture behaviour of thermally modified Scots pine (*Pinus sylvestris* L.) wood. *J. Mater. Sci*. 51(3):1–8.

Chen, G., H. Luo, H. Yang, T. Zhang, and S. Li. 2017. Water effects on the deformation and fracture behaviors of the multi-scaled cellular fibrous bamboo. *Acta Biomater*. 65:203–215.

Chen, M., L. Ye, G. Wang, C. Fang, C. Dai, and B. Fei. 2019. Fracture modes of bamboo fiber bundles in three-point bending. *Cellulose* 26:8101–8108.

Christoforo, A. L., V. B. de Moura Aquino, J. S. Govone, A. M. P. G. Dias, T. H. Panzera, and F. A. R. Lahr. 2020. Alternative model to determine the characteristic strength value of wood in the compression parallel to the grain. *Maderas-Cienc. Tecnol*. 22(3). DOI:10.4067/20718-221X2020005000303

Esteban, L. G., C. Simón, F. G. Fernández, P. de Palacios, R. M. Sampedro, M. E. Eugenio, and R. Hosseinpourpia. 2015. Juvenile and mature wood of *Abies pinsapo* Boissier: Sorption and thermodynamic properties. *Wood Sci. Technol*. 49(4):725–738.

Habibi, M. K. and Y. Lu. 2014. Crack propagation in bamboo's hierarchical cellular structure. *Sci. Rep*. 4:5598.

Hanlon, T., E. D. Tabachnikova, and S. Suresh. 2005. Fatigue behavior of nanocrystalline metals and alloys. *Int. J. Fatigue* 27(10–12):1147–1158.

Hill, C. A. S, A. Norton, and G. Newman. 2009. The water vapor sorption behavior of natural fibers. *J. Appl. Polym. Sci*. 112(3):1524–1537.

Hill, C. A. S., J. Ramsay, B. Keating, K. Laine, L. Rautkari, M. Hughes, and B. Constant. 2012. The water vapour sorption properties of thermally modified and densified wood. *J. Mater. Sci*. 47(7):3191–3197.

Irby, N. E., F. J. N. França, H. M. Barnes, R. D. Seale, and R. Shmulsky. 2020a. Effect of growth rings per inch and density on compression parallel to grain in southern pine lumber. *BioResources* 15(2):2310–2325.

Irby, N. E., F. J. N. França, H. M. Barnes, R. D. Seale, and R. Shmulsky. 2020b. Effect of growth rings per inch and specific gravity on compression perpendicular to grain in No. 2: 2 by 8 and 2 by 10 southern pine lumber. *Forest Prod. J*. 70(2):213–220.

Keating, B. A., C. A. S. Hill, D. Sun, R. English, P. Davies, and C. McCue. 2013. The water vapor sorption behavior of a galactomannan cellulose nanocomposite film analyzed using parallel exponential kinetics and the Kelvin–Voigt viscoelastic model. *J. Appl. Polym. Sci*. 129(4):2352–2359.

Liese, W. and J. Walter. 2003. Bamboo and rattan in the world. *J. Bamboo Rattan* 2(2):189–189.

Liu, X., G. Tian, L. Shang, S. Yang, and Z. Jiang. 2014b. Compression properties of vascular boundless and parenchyma of rattan (*Plectocomia assamica* Griff). *Holzforschung* 68:927–932.

Liu, X. E., W. H. Lv, and Y. X. Zheng. 2014a. Influence of moisture content on the bending properties of rattan cane. *J. Anhui Agric. Univ*. 41(6):934–938. (Translated from Chinese.)

Liu, Y. Q. and G. J. Zhao. 2004. Wood Resource Materials Science. China Forestry Publishing, Beijing. (In Chinese.)

Lu, Y. and J. J. Pignatello. 2004. History-dependent sorption in humic acids and a lignite in the context of a polymer model for natural organic matter. *Environ. Sci. Technol*. 38(22):5853–5862.

Luo, Z., X. Zhang, B. Lu, B. Pan, and Z. Ruan. 2012. Mechanical properties and test methods of rattan. *Furn. Inter. Décor* 7:108–110.

Obataya, E., P. Kitin, and H. Yamauchi. 2007. Bending characteristics of bamboo (*Phyllostachys pubescens*) with respect to its fiber foam composite structure. *Wood Sci. Technol*. 41:385–400.

Olek, W., J. Majka, and L. Czajkowski. 2013. Sorption isotherms of thermally modified wood. *Holzforschung* 67(2):183–191.

Rich, P. M. 1986. Mechanical architecture of arborescent rain forest palms. *Principes* 30:117–131.

Shang, L. L. 2014. The Research on Fundamental Properties and Toughening Modification of *Plectocomia kerrana*. Chinese Academy of Forestry, Beijing. (In Chinese.)

Simpson, W. T. and A. TenWolde. 1999. Physical properties and moisture relations of wood, chap. 3. *In:* Wood Handbook: Wood as an Engineering Material. Forest Products Laboratory, Madison, Wisconsin. 55 pp.

Skaar, C. 1988. Wood–Water Relations. Springer-Verlag, Berlin. 283 pp.

Standardization Administration of China (SAC). 2009. Method of testing in compressive strength parallel to grain of wood. GB/T 1935–2009. *In:* SCSF. Wood. SAC, Beijing.

Tiemann, H. D. 1906. Effect of moisture upon the strength and stiffness of wood. USDA Forest Service Bulletin 70. Government Printing Office, Washington, D.C.

Valentin, G. and G. Adjanohoun. 1992. Applicability of classical isotropic fracture mechanics specimens to wood crack propagation studies. *Mater. Struct*. 25:3–13.

Verbist, M., J. M. Branco, and L. Nunes. 2020. Characterization of the mechanical performance in compression perpendicular to the grain of insect-deteriorated timber. *Buildings* 10(1):14.

Walker, J. 2006. Water in wood. *In:* Primary Wood Processing. Principles and Practice. 2nd ed. Springer Verlag, Dordrechtthe, the Netherlands. pp. 69–94.

Wang, K., X. E. Liu, L. L. Shang, J. F. Ma, and G. L. Tian. 2019. The variations of anatomical microstructure of *Calamus simplicifolius* during development. *Wood Process. Machin*. 30(1):17–20. (Translated from Chinese.)

Wang, K. L. 2015. Resources and distribution of rattan in China. *Plant Sci. J*. 33(3):320–325. (Translated from Chinese.)

Xie, Y., C. A. S. Hill, Z. Jalaludin, S. F. Curling, R. D. Anandjiwala, A. J. Norton, and G. Newman. 2011. The dynamic water vapour sorption behaviour of natural fibres and kinetic analysis using the parallel exponential kinetics model. *J. Mater. Sci*. 46(2):479–489.

Youssefian, S. and N. Rahbar. 2015. Molecular origin of strength and stiffness in bamboo. *Fibrils Sci. Rep*. 5:11116.

Zhang, X., J. Li, Z. Yu, Y. Yu, and H. Wang. 2017. Compressive failure mechanism and buckling analysis of the graded hierarchical bamboo structure. *J. Mater. Sci*. 52(12):6999–7007.